

## Numerical Simulation of Volcanomagnetic Effects due to Hydrothermal Activity

Ayako OKUBO, Wataru KANDA and Kazuhiro ISHIHARA

### Synopsis

We have developed a postprocessor to calculate the geomagnetic field variations caused by hydrothermal activities in the volcanic region. They use distributions of temperature inside the volcano, which are results of a numerical simulation for hydrothermal activity after magma intrusion. The most dominant mechanism of volcanomagnetic effects was considered here: thermomagnetic effect. We examined the influences of host rock permeability and depth of magma intrusion on thermomagnetic effect. Results showed that the shallower depth of intrusion causes larger total intensity anomaly and earlier decline of it and that larger anomalies appear at later times in cases of lower permeability host rocks.

**Keywords:** hydrothermal activity, thermomagnetic effect, numerical simulation, magma intrusion, permeability.

### 1. Introduction

Continuous observations of geomagnetic total intensity have been carried out on many active volcanoes (e.g., Tanaka, 1993; Del Negro et al., 2000). Those observations are aimed mainly to know thermal condition of the shallow volcanic edifice because thermal demagnetization or remagnetization of the volcanic rocks occurs if the volcano is considerably heated or cooled, which could be observed as the geomagnetic field variations on the ground. In addition to this thermomagnetic effect, two mechanisms are widely accepted for the geomagnetic field changes associated with volcanic activities. One is piezomagnetic effect which is related to stress-induced changes in rock magnetization and the other is electrokinetic effect which arises from motion of electric charges associated with fluid flow within the volcanic edifice. Thus, volcanomagnetic effects could provide various kinds of information to understand the volcanic activity. However, the observed geomagnetic field changes have been interpreted, in many cases, as thermomagnetic effect, because it generally yields larger changes than other two mechanisms and because it is difficult to discriminate

each effect from the observed data.

Conventionally, the geomagnetic field differences between the observation sites and a reference site in a certain period are explained by using a very simplified model that assumes an equivalent magnetic dipole, in order to estimate the thermally anomalous region. However, this method involves following problems for the interpretation of the observed data. Firstly, the estimated anomalous region is rough in temporal and spatial scale because the data is integrated. Even if the rate of the geomagnetic field change varies, the obtained model does not reflect it because the data is treated as an amount of the site difference in a period. Secondly, there is no temporal and spatial continuity in the model. Especially, when the available observation sites are few, an inconsistent result that the demagnetized area at a certain temporal "A period" is far apart from the area at the next "B period" can be obtained. Thirdly, the volcanological interpretation is "Dated": spatio-temporal variations of heat, stress, and rock properties associated with hydrothermal activities should be considered. These problems originate in the fact that the majority of the observed time series data is not used. It is insufficient to discuss quantitatively the relation to the volcanic

activity by the conventional thermomagnetic interpretation.

In this study, we consider hydrothermal fluid flows as a factor to change the physical state within the volcanic edifice and evaluate numerically the geomagnetic field changes based on the temperature and pressure distribution inside the volcano. In this paper, we focused on thermomagnetic effect as a first step of the study.

## 2. The postprocessor

Our calculation utilizes a hydrothermal fluid flow simulation inside the volcano. We used the numerical simulation code HYDROTHERM (Hayba and Ingebritsen, 1994) for this purpose. The code gives the temperature distribution at each time step, so that a magnetic field change due to temperature-dependent rock magnetization ( $J$ ) is considered as a post-processor.

Ishido and Pritchett (2001) formulated the temperature dependence of the magnetization based on the laboratory experiment of the remanent magnetism for rocks sampled at Izu-Oshima volcano. We adopted this formulation here. The pertinent parameters are temperatures  $T_1$  and  $T_2$  (with  $T_1 < T_2$ ) and rock magnetization per unit volume  $M_0$ . The magnetization per unit volume is taken to be equal to  $M_0$  so long as the temperature ( $T$ ) is less than  $T_1$  and equal to zero if  $T$  exceeds  $T_2$ . For intermediate temperatures,

$$J = M_0 \times (1 - 3\eta^2 + 2\eta^3) \quad (1)$$

where  $\eta = (T - T_1)/(T_2 - T_1)$ . In this paper,  $M_0 = 5 \text{ A/m}$ ,  $T_1 = 100^\circ\text{C}$ , and  $T_2 = 600^\circ\text{C}$  are given. It is also assumed that the direction of the initial magnetization is the same as that of the geomagnetic field (inclination of  $45^\circ$  and declination of  $0^\circ$ ). Rock magnetization at any point in the computation domain is calculated from the temperature distribution that is obtained from the hydrothermal fluid simulation.

Next, the magnetic total intensity at an observation site is estimated. Generally, the magnetic field  $g_i$  at site  $i$  is written as

$$g_i = \sum \omega_{ij} \cdot J_j, \quad (2)$$

where  $\omega_{ij}$  indicates the magnetic field at  $i$ -th observation site due to  $j$ -th magnetic source with unit magnetization, and  $J_j$  is the magnetization of  $j$ -th source. In this calculation, we used a different grid of numerical discretization from that used in HYDROTHERM in order to reduce the terrain effect. The explicit form of  $\omega_{ij}$

was obtained by using the technique of Sasai (1991) based on the circular cone model of Rikitake (1951).

Finally, the anomalous total intensity is obtained as the difference between  $g_i$  and  $g_{i0}$  where  $g_{i0}$  indicates the total intensity at the stationary state of the hydrothermal activity.

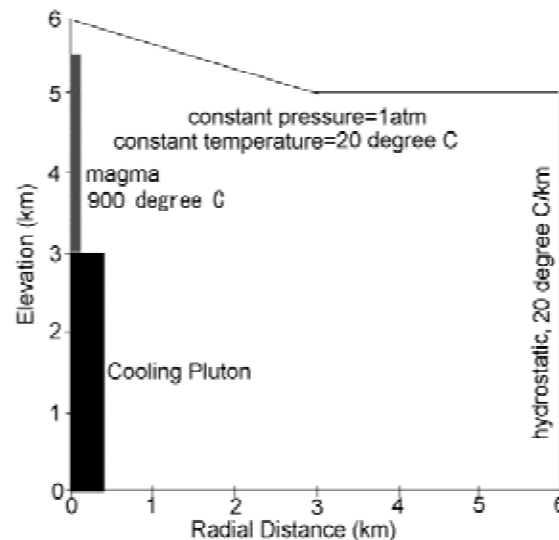


Fig. 1 Geometry and boundary conditions of the model used for all simulation presented in this study. Initial temperature of the shallow magma intrusion is assumed as  $900^\circ\text{C}$ .

## 3. The numerical model

The configuration of the numerical model is shown in Fig. 1. A 2-D axis-symmetric coordinate system was used to simulate a 3-D cylindrical domain. Simulation begins with the instantaneous intrusion of a  $900^\circ\text{C}$  pluton upto the 3 km deep with a radius of 400 m. After the pluton is sufficiently cooled (30,000 years later), a fresh magma with a radius of 40 m newly intrudes from the top of the cooling pluton. Various model parameters including properties of volcanic rocks as well as initial and boundary conditions are similar to those used by Hayba and Ingebritsen (1997).

The ground surface has a specified hydraulic head equal to its elevation with a constant fluid pressure of 0.1013 MPa (1 atm) and temperature of  $20^\circ\text{C}$ . The right-hand boundary, located 5 km away from the center of the edifice, holds initial hydrostatic pressure and temperature with a vertical gradient of  $20^\circ\text{C/km}$  and allows lateral flows of fluid and heat. The bottom boundary is impermeable, with a constant basal heat flux of  $80 \text{ mW/m}^2$  into the host rock and a constant flux of

120  $mW/m^2$  into the pluton. The left-hand boundary represents an axis of symmetry, so that it is impermeable and insulating. We also specify that initial pressure within the pluton and magma are 10% less than lithostatic pressures.

As for rock properties, we assumed temperature dependent intrinsic permeability and heat capacity, while other rock properties (porosity, density, and heat capacity) were constant throughout the simulations (Table 1). At temperature above 500 °C, permeability is negligibly low of  $10^{-22} m^2$  (both host-rock and magma). As temperature decreases from 500 to 400 °C, permeabilities increase log-linearly to  $10^{-19} m^2$  for magma and  $10^{-17} m^2$  for host-rock. As temperature decreases further to 360 °C, host-rock permeabilities of  $10^{-12}$ - $10^{-14} m^2$  and the magma of  $10^{-18} m^2$  are assumed (c.f. Manning and Ingebritsen, 1999). The cooling pluton also holds low permeability ( $10^{-18} m^2$ ) throughout its entire history. We adopted the approach of Hanson and Barton (1989) for the temperature dependence of rock heat capacity. It is normally 2000  $J/(kg K)$  for both magma and host rock and doubled for temperatures between 900 °C and 750 °C.

The calculation domain was discretized into 40 (vertical direction labeled as  $z$ ) x 30 (horizontal direction labeled as  $x$ ) blocks. The grid spacing in the  $x$  direction was 10 m ( $0 < x < 200$ ), 200 m ( $200 < x < 400$ ), 100 m ( $400 < x < 500$ ), 250 m ( $500 < x < 1000$ ), 500 m ( $1000 < x < 3000$ ), and 1500 m ( $3000 < x < 6000$ ). In the  $z$  direction, it was 500 m ( $0 < z < 1500$ ), 250 m ( $1500 < z < 3000$ ), 100 m ( $3000 < z < 5900$ ), 99m ( $5900 < 5999$ ), and 1m ( $5999 < z < 6000$ ).

Table 1 Rock Properties. Details of  $f(T)$  and  $g(T)$  are described in the text.

Property	Pluton	Host rock
Permeability $m^2$	$f(T)$	$f(T)$
Porosity %	5	10
Heat capacity $J/(kg K)$	$g(T)$	$g(T)$
Thermal conductivity $W/(m K)$	2	2
Rock density $kg/m^3$	2500	2500

#### 4. Hydrothermal circulation and anomalies in geomagnetic total intensity

Fig. 2 shows the evolving temperature and fluid-flow patterns near intrusion of the magma for *Model A* (Table 2). The corresponding anomalies in geomagnetic total

intensity are shown in Fig.3. Just after the intrusion, steam appears in the upper part of the intruded magma, although flow patterns at outside of the magma are not disturbed yet by intrusion (Fig.2a). High temperature zone is restricted to the vicinity of the magma and steep gradient is seen at the interface between magma and the host. The anomalous geomagnetic field distribution caused by high temperature magma intrusion is obtained (Fig.3a). During 8 years to 16 years after the intrusion (Fig.2b and 2c), a strong upward flow occurs at deeper part just outside of the magma. The vapor zone also extends outward as well as downwards along the interface, which results in the appearance of two-phase zone. Hydrothermal circulation is arising. High temperature zone extends gradually near the upper part of the magma. Pattern of the anomalous geomagnetic field is similar to that obtained in the previous time step, although amounts of the anomaly are considerably larger (Fig.3b and 3c). At 32 years after the intrusion (Fig.2d), the well-developed hydrothermal circulation is seen. However, the temperature of the magma decreases to 600-700 °C because the heat is transported by the intense fluid flows. Accordingly, vapor zone reaches down to the bottom of the intruded magma at the interface. The largest anomaly of the geomagnetic field is observed at this time step (Fig.3d). Hydrothermal circulation extends laterally and high temperature zone extends to the corresponding area, although magma is cooled down to about 400 °C where vapor zone is dominant at 64 years after the intrusion (Fig.2e). The magnetic anomaly at this time step (Fig.3e) shows nearly the same pattern as that shown in Fig.3d but slightly small anomalies are obtained. At 128 years after the intrusion, heat of the intruded magma is almost discharged and fluid flow pattern goes to the steady state (Fig.2f). The anomalous geomagnetic fields are disappearing (Fig.3f).

Table 2 Four models used in the case studies for thermomagnetic effect caused by hydrothermal activity.

Model	host rock permeability (< 360 °C)	Top depth of the intruded magma
<i>Model A</i>	$10^{-13} m^2$	500 m (a.s.l.)
<i>Model B</i>	$10^{-13} m^2$	0 m (a.s.l.)
<i>Model C</i>	$10^{-12} m^2$	500 m (a.s.l.)
<i>Model D</i>	$10^{-14} m^2$	500 m (a.s.l.)

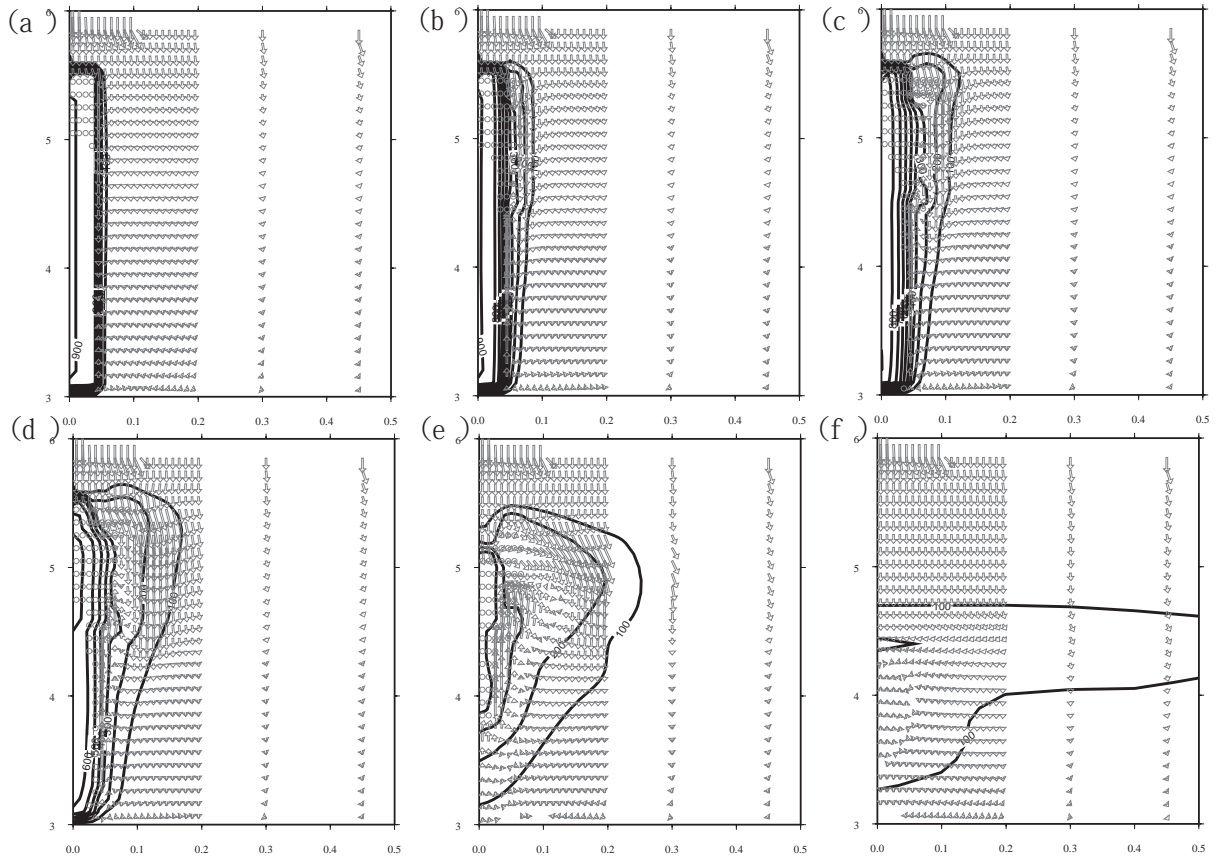


Fig. 2 Simulation results for *Model A* showing temperature contours and fluid-flow vectors at selected times after a fresh magma intrusion: (a) 1 yr, (b) 8 yr, (c) 16 yr, (d) 32 yr, (e) 64 yr and (f) 128 yr. Arrows represent flow vectors for liquid and supercritical water. Circles show that the fluid is vapor (steam).

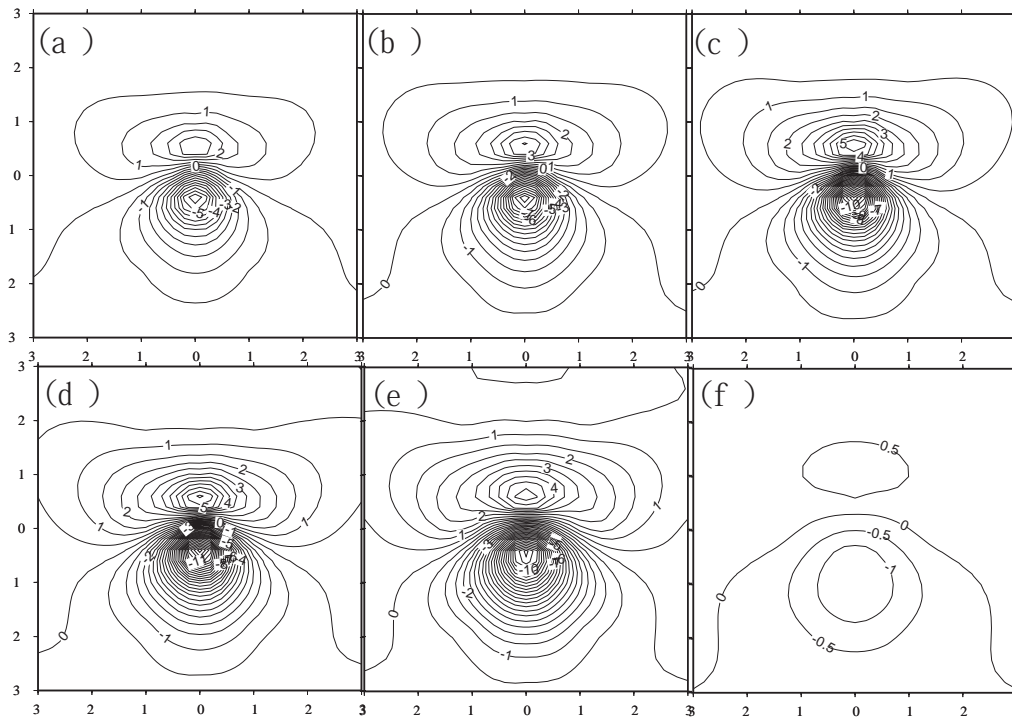


Fig. 3 Corresponding anomaly map of the calculated changes in total intensity caused by the fresh magma intrusion shown in Fig. 2: (a) 1 yr, (b) 8 yr, (c) 16 yr, (d) 32 yr, (e) 64 yr and (f) 128 yr after the intrusion. Area shows -3.0 to +3.0 km in East direction and -3.0 to +3.0 km in North direction. Contour intervals are 0.5 nT.

## 5. Case studies

We examined the influences of host rock permeability and depth of the magma intrusion. Four models shown in Table 2 were simulated compared.

### 5.1 Influence of the depth of magma intrusion

Fig. 4 shows North-South profiles of anomalous geomagnetic total intensity for different depths of the magma intrusion. Host rock permeability is the same (Table 2). In comparison with Fig. 4(b), Fig. 4(a) shows larger anomalies at all the time steps, although the anomalous areas are smaller. In addition, the peak of the anomaly reaches its maximum at 32 years after the intrusion for *Model A* as also shown in Fig.3, while the maximum peak is seen at 64 years after the intrusion for *Model B*. This indicates that the shallower depth of intrusion causes larger total intensity anomaly and earlier decline of it. As shown in Fig.2, hydrothermal circulation develops near the upper part of the intruded magma and extends laterally as time goes. These results suggest that the larger hydrothermal circulation is developed in the shallower magma intrusion model. Since the larger volumes of the fluid advect heat, the hydrothermal circulation declines earlier.

### 5.2 Influence of host rock permeability

The geomagnetic field changes shown in Fig. 5 summarize the thermomagnetic effect for different permeabilities at two selected sites. Those sites are located north (0 m Easting, 500 m Nothing) and south (0 m Easting, -500 m Northing) from the center, at which decreasing and increasing centers of the anomaly are observed for the case of *Model A* (Fig.3). Simulation results for two models with one-order higher (*Model C*) and lower (*Model D*) permeabilities are compared with the result for *Model A*. The top depth of the intruded magma is the same for all models (Table 2).

We can see two features in Fig.5. One is that higher permeability of the host rock results in shorter duration of the geomagnetic field anomalies. This is because advective heat transport dominates in the higher permeability host. The larger volumes of the fluid rapidly advect heat from the magma, so that the hydrothermal circulation is not maintained for a long time.

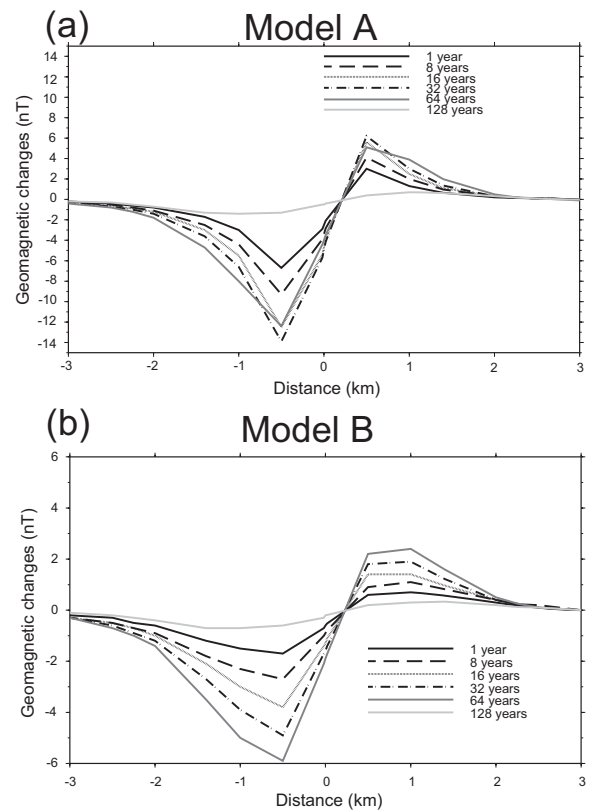


Fig. 4 North-South profiles of anomalous total intensity for different depths of the magma intrusion: (a) *Model A* (500 m a.s.l.) and (b) *Model B* (0 m a.s.l.). Six profiles at different time steps after the intrusion ( $2^0$  yr,  $2^3$  yr,  $2^4$  yr,  $2^5$  yr,  $2^6$  yr, and  $2^7$  yr) are shown in each figure.

The other feature in Fig. 5 is that lower permeability yields larger anomalies in geomagnetic total intensity, although the anomalies obtained by three models just after the intrusion are nearly the same. The initial anomalies are caused by the direct influence of the high temperature magma, which are the same for three models. However, anomalies obtained by models with lower permeability hosts (*Model A* and *D*) show gradual increase at site north and decrease at site south. This means that demagnetized zone, that is, high temperature zone expands widely and is caused by hydrothermal circulation (see Fig.2). Since the effect of advective heat transport is less for the lower permeability models, it takes longer time to cool down the intruded magma. Consequently, hydrothermal circulation is maintained for a long time

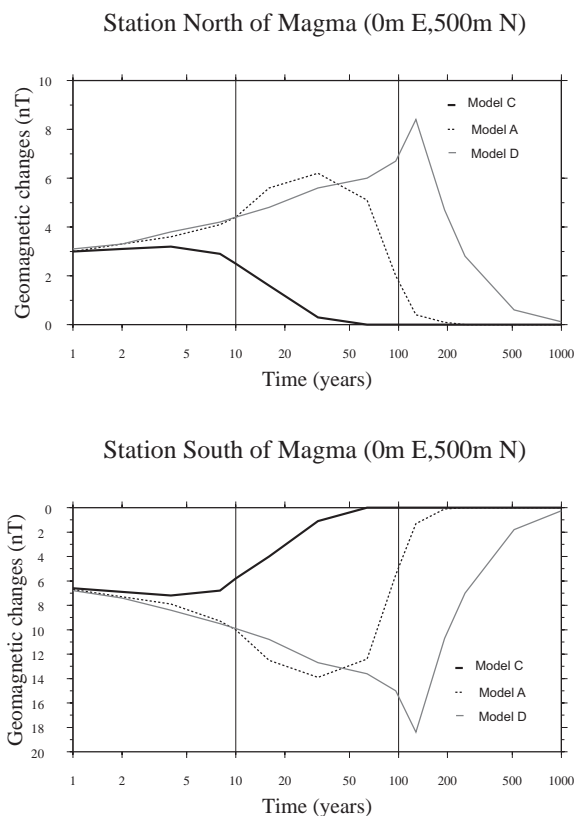


Fig. 5 Histories of anomalous total geomagnetic intensity caused by a fresh magma intrusion into various permeabilities of host rocks: *Model C* ( $10^{-12} \cdot \text{m}^2$ ), *Model A* ( $10^{-13} \cdot \text{m}^2$ ), and *Model D* ( $10^{-14} \cdot \text{m}^2$ ).

## 6. Conclusions

We calculated spatio-temporal variations of the thermomagnetic effect caused by hydrothermal activity driven by the intruded magma. We utilized HYDROTHERM (Hayba and Ingebritsen, 1994) for the fluid flow simulation after the magma intrusion and developed a postprocessor to calculate the anomalous geomagnetic total intensity. We examined the influences of host rock permeability and depth of magma intrusion. Following results were obtained in this study:

1. The depth of magma intrusion influences not only the amount of total intensity changes but also the duration of the anomalous geomagnetic field. The shallower depth of intrusion causes larger total intensity anomaly and earlier decline of it.

2. Host rock permeability strongly affects both the duration of the anomalous geomagnetic field and the amount of it. In the case of lower permeability hosts, larger anomalies appear at later times because advective

heat transfer is less and hydrothermal circulation is maintained in a wider area for a longer time.

## Acknowledgements

The authors are grateful to Y. Sasai of, Tokyo Metropolitan Government and T. Ishido of Geological Survey of Japan. for useful discussions and helpful criticism.

## References

- Del Negro, C. and Ferrucci, F. (2000): Volcanomagnetic effects at Vulcano Island (Aeolian archipelago, Italy), *Geophys. J. Int.*, Vol. 140, pp. 83-94.
- Hanson, R. B. and Barton, M. D. (1989): Thermal development of low-pressure metamorphic belts: Results from two-dimensional numerical models, *J. Geophys. Res.*, Vol. 94, 10363-10377.
- Hayba, D. O. and Ingebritsen, S. E. (1994): The computer model HYDROTHERM, a three-dimensional finite-difference model to simulate ground-water flow and heat transport in the temperature range of 0 to 1,200 °C, U. S. Geol. Surv. Water Resour. Invest. Rep., No. 94-4045, 85 pp.
- Hayba, D. O. and Ingebritsen, S. E. (1997) Multiphase groundwater flow near cooling plutons, *J. Geophys. Res.*, Vol. 102, pp. 12235-12252.
- Ishido T. and Pritchett J. W. (2001): Prediction of magnetic field changes induced by geothermal fluid production and reinjection, *GRC Transactions*, Vol. 25, pp. 645-649.
- Manning, C. E. and Ingebritsen, S. E. (1999): Permeability of the continental crust: Implications of geothermal data and metamorphic systems, *Rev. Geophys.*, Vol. 37, pp. 127-150.
- Rikitake, T. (1951): The distribution of magnetic dip in Ooshima (Oo-sima) Island and its change that accompanied the eruption of Volcano Mihara, 1950, *Bull. Earthq. Res. Inst.*, Vol. 29, pp. 161-181.
- Sasai, Y. (1991): Integrals of Lipschitz-Hankel type for solving potential problems with axial symmetry, *Proc. Conductivity Anomaly Workshop*, pp. 110-121.
- Tanaka, Y. (1993) Eruption mechanism as inferred from geomagnetic changes with special attention to the 1989-1990 activity of Aso volcano, *J. Volcanol. Geotherm. Res.*, Vol. 56, pp. 319-338.

## 熱水流動を考慮した火山体磁化構造時間変化モデル

大久保綾子・神田径・石原和弘

### 要旨

マグマ貫入後の熱水流動のシミュレーションを行い、熱水系の消長によって地表での地磁気がどのように変化するかを数値的に評価した。シミュレーションで得られる温度分布から火山体内部の磁化分布を見積もり、地表での地磁気変化を計算するポストプロセッサーを開発し、マグマの貫入の深さおよび浸透率が地磁気変化に与える影響を調べた。その結果、より浅くマグマが貫入する方が、地磁気変化が大きく、地磁気変化が観測される時間が短いこと、また、浸透率が小さい方が、地磁気変化が大きく、地磁気変化が観測される時間が長いことがわかった。

**キーワード:** 熱水流動, 熱磁気効果, シミュレーション, マグマ貫入, 浸透率